curvature effects predominate. Aposteriori evaluation of the other two assumptions will provide an estimation of their importance.

In addition, the shock shape must be known. For sphere-cones, the shock correlation of Ref. 3 is

$$\frac{y}{\cos\theta_c} = 1.424\left[C_D^{1/2}\frac{x}{\cos\theta_c}\right]^{0.46} \tag{8}$$

which is faired into the conical shock angle given by the correlation

$$\sin\theta_{cs} = 1.01\sin\theta_c + (0.536/M_\infty) \tag{9}$$

The tangent point is

$$\frac{y}{\cos\theta_c} = \left[\frac{0.984C_D}{\tan^2\theta_{cs}}\right]^{0.426} \tag{10}$$

To apply the method, the properties immediately behind the shock are determined for several values of y up to the straight portion of the shock. Expanding these conditions isentropically to the assumed constant sphere-cone pressure, the boundary-layer edge parameters are determined for some unknown s. The shock wave and isentropic expansion calculations can be done for either perfect or real gases; however, the calculations of this note are confined to the perfect gas case. These values are used to calculate $\phi_T(y)$ from Eq. (6). Then,

$$\int_0^s r^{5/4}ds = \int_0^y \phi_T(y)dy \tag{11}$$

Since, for sphere cones,

$$r = \cos\theta_c + \left(s - \frac{90 - \theta_c}{180}\pi\right)\sin\theta_c \tag{12}$$

the left side of Eq. (11) can be integrated directly to yield finally

$$r^{9/4} = \left(\cos\theta_c - \frac{90 - \theta_c}{180}\pi\sin\theta_c\right)^{9/4} + \frac{9\sin\theta_c}{4}\int_0^y \phi_T(y)dy \tag{13}$$

which is easily solved for r and thus s.

The preceding equations were applied to a 15° half-angle sphere-cone with a 3-in. nose radius at an altitude of 50,000 ft and a Mach number of 20. C_m was taken equal to 1. Figure 1 shows the variation of boundary-layer edge Mach number along the body for a perfect gas. The conical value is attained at an actual surface location of about 79 in. Examination of Eq. (6) shows that the nose radius effect is simply a multiplicative constant. Thus, if the nose radius is halved, the conical Mach number is reached at an actual surface location of 36 in., a considerable effect. For perfect gas calculations, the altitude effect is also confined to the constant, and changing the altitude to 100 kft reduces the conical Mach number location to 59 in., a smaller but still significant change. Thus, as expected, decreasing the nose radius and increasing the altitude compound the shock curvature problem.

The effects of the assumption of constant C_m and the variation of ρ^*/ρ_e over the body were evaluated aposteriori. The

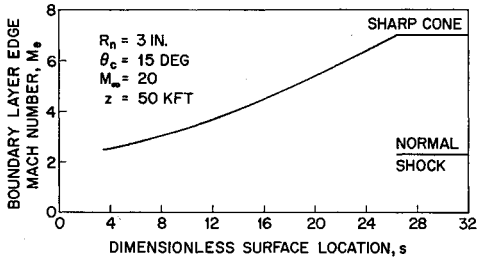

Fig. 1 The distribution of boundary-layer edge Mach number along a sphere-cone.

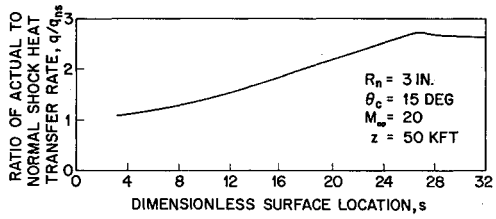

Fig. 2 The distribution of cold wall turbulent heat-transfer rate along a sphere-cone.

cold wall value of C_m varied less than 25% from the conical value to that for boundary-layer edge emanation from a normal shock. The average value was slightly greater than 1. This variation increased the surface location at which cone flow began by less than 3%. Evaluating the second term in the brackets of Eq. (6) caused a decrease of less than 10% in the surface location at which cone flow was established. The two effects are of opposite sign for the present case, thus minimizing their importance. Although the effect of the present assumptions are not insignificant, it is felt that meaningful results can still be obtained.

The cold wall heat-transfer rate, normalized to that expected for boundary-layer edge emanation from a normal shock, is presented in Fig. 2. Although increases of 30 to 40% in heat-transfer rate are expected for a similar laminar case,[1] the turbulent results indicate factors of from 2 to 3. This effect should be easily discernible (unlike the smaller laminar effect) in experimental data. Unfortunately, few turbulent data exist for sphere-cones. The magnitude of the values herein emphasize the need for such data.

References

[1] Rubin, I., "Shock curvature effects on the outer edge conditions of a laminar boundary layer," AIAA J. 1, 2850–2852 (1963).

[2] Bromberg, R., Fox, J. L., and Ackermann, W. G., "A method of predicting convective heat input to the entry body of a ballistic missile," Ramo-Woolridge Corp., Los Angeles, Calif. (June 1956); confidential.

[3] Klaimon, J. H., "Bow shock correlation for slightly blunted cones," AIAA J. 1, 490–491 (1963).

Improved Calculation of Vacuum Vertical Trajectories

Leo B. Schlegel* and Philip J. Bonomo*
International Business Machines Corporation, Bethesda, Md.

Introduction

In preliminary trajectory analysis, vacuum vertical trajectories are often employed as approximations or limiting cases. Examples are idealized sounding rocket trajectories, lunar landing descent paths, limiting minimum time transfers between coplanar circular orbits, etc. When the over-all altitude variation for such a trajectory is small, the approximation of constant gravitational acceleration is usually made to facilitate calculation of velocity and altitude time histories. At modest additional effort, however, these calculations can be based on an inverse-square gravity field and hence made more nearly exact. The appropriate formulation is a limiting version of Lambert's theorem for transfer time between two radii on a Keplerian ellipse, a vacuum vertical trajectory being

Received April 13, 1964; revision received May 8, 1964.

* Advisory Engineer, Federal Systems Division. Member AIAA.

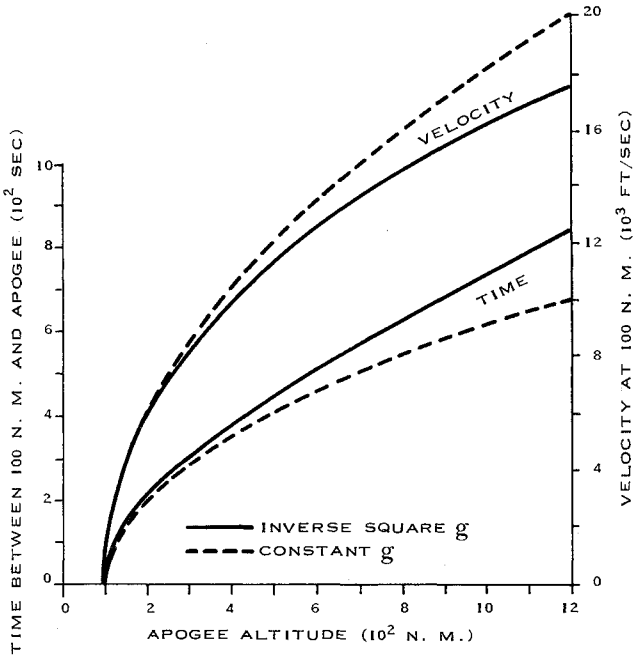

Fig. 1 Vertical trajectory data: earth.

a degenerate case of such an ellipse. This approach is implicit in both the rectilinear motion equations of Moulton[1] and the derivation of Lambert's theorem given by Battin,[2] but is still somtimes overlooked in current studies.

This note summarizes the simplified Lambert equations for vertical trajectories in vacuo, and compares typical velocity and flight time data for constant-g and inverse-square-g paths in earth and moon gravity fields. The altitude range beyond which a constant-g approximation yields unacceptable accuracies may thus be estimated.

Equations

Lambert's theorem for transfer time t between initial and final radii r_0 and r on a Keplerian ellipse of semimajor axis a about gravity center μ is given by (e.g., see Sconzo[3])

$$t = a^{3/2}\mu^{-1/2}[(\alpha - \sin\alpha) - (\beta - \sin\beta)] \tag{1}$$

where

$$\sin(\alpha/2) = [(r_0 + r + c)/4a]^{1/2}$$
$$\sin(\beta/2) = [(r_0 + r - c)/4a]^{1/2} \tag{2}$$

and c is chord length between the radius vectors. For a vertical trajectory specified by initial conditions r_0 and $\dot{r}_0$, c is simply the (positive) difference between r_0 and r, and a is obtained from solution of the standard vis-viva relation of orbital mechanics:

$$\dot{r}_0^2 = \mu[(2/r_0) - (1/a)] \tag{3}$$

Although these simplifications considerably shorten the evaluation of (1) and (2), it is often more convenient in practice to refer all calculations to the zero-velocity point at "apogee" of the trajectory, and this is the approach to be outlined here. Apogee radius r_a and the corresponding time between r_0 and r_a are usually also of interest in themselves, so that apogee is a natural choice as reference point. With apogee established, vertical flight time between r_0 and r is easily obtained as the difference in times between each of these radii and apogee. Particularly simple forms for (1) and (2) are available for these calculations. Thus, putting $a = r_a/2$ (perigee radius is zero for a vertical trajectory), $r = r_a$, and $c = r_a - r_0$ in (1) and (2), the time between r_0 and r_a is

$$t = (r_a/2)^{3/2}\mu^{-1/2}(\pi - \beta + \sin\beta)$$
$$\text{where } \sin(\beta/2) = (r_0/r_a)^{1/2} \tag{4}$$

Equations (4), with r_0 replaced by r, equally well express the time between a general r and r_a. Finally, introducing a new variable $\psi = \pi - \beta$ in (4), Lambert's equation for the time between any r and r_a reduces to

$$t = (r_a/2)^{3/2}\mu^{-1/2}(\psi + \sin\psi)$$
$$\text{where } \cos(\psi/2) = (r/r_a)^{1/2} \tag{5}$$

This development is valid for both ascending and descending trajectories, since the velocity magnitudes and altitude time histories of each are images about apogee.

Examples

To illustrate one application of (5), Fig. 1 shows the vacuum vertical transfer time between 100-naut-mile earth altitude and apogee, as a function of apogee, for an extended range of sounding rocket altitudes. The corresponding initial velocity at 100 naut miles to attain the apogee altitudes indicated is computed from (3) and included for reference. Also shown are the same time and velocity data based on a constant-g approximation, where the constant value employed is g at 100-naut-mile altitude. The errors introduced by constant g are appreciable for the higher altitudes. For example, beyond 1000-naut-mile apogee, initial velocity and total flight time errors exceed 1800 fps and 120 sec, respectively; both these errors are greater than 10% of the true (i.e., nonconstant-g) values. Of course, some reduction is possible by using for constant g a value belonging to an intermediate altitude between start and terminus.

As another example, Eq. (5) and the general form of (3), with r and $\dot{r}$ replacing r_0 and $\dot{r}_0$, are used to generate the altitude and velocity time history data of Fig. 2 for a vertical descent to the moon starting from rest at 200-naut-mile altitude. Such a trajectory approximates a nearly complete deboost from lunar orbit, followed by a short central angle descent arc to the start of a braking maneuver at low altitude. As noted previously, transfer times between intermediate altitudes can be found by differencing the separate times from apogee to those altitudes. Comparison with the corresponding constant-g data (based on lunar g at zero altitude) shows a difference in final velocity and flight time of about 300 fps and 120 sec, respectively, again more than 10% error. The constant-g approximation is thus seen to give about the same percentage error over a smaller altitude regime for the moon

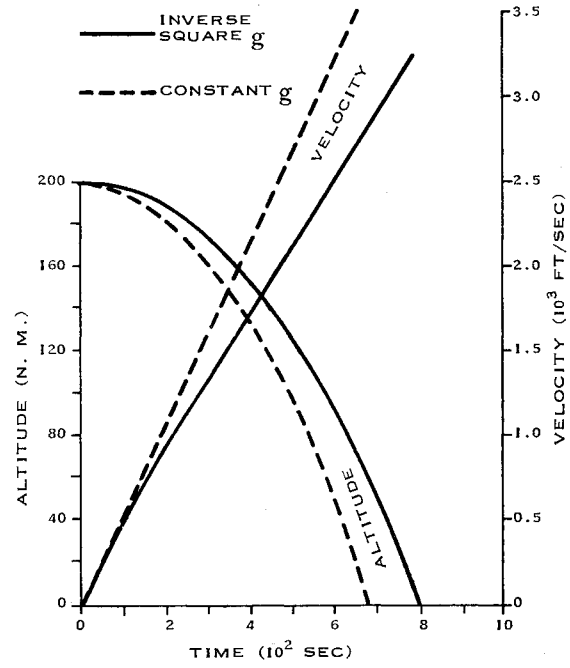

Fig. 2 Time history of vertical descent from 200 naut miles to lunar surface.

than for earth. This follows because of the greater percentage change in lunar gravitational acceleration compared to that of earth over a given altitude increment, and points up the need for special care in applying a constant-g approximation for lunar vertical trajectories.

References

[1] Moulton, F. R., *An Introduction to Celestial Mechanics* (Macmillan Co., New York, 1914), 2nd revised ed., pp. 43–45.

[2] Battin, R. H., "The determination of round-trip planetary reconnaissance trajectories," Massachusetts Institute of Technology Instrumentation Lab. Rept. R-219 (January 1959).

[3] Sconzo, P., "The use of Lambert's theorem in orbit determination," Astron. J. **67**, 19–21 (1962).

Rapid Estimation of the Far-Field in an Axisymmetric Compressible Jet

RICHARD S. ROSLER*
United Technology Center, Sunnyvale, Calif.

IT is of interest to be capable of rapidly estimating the far field characteristics of free jets. Hence, the somewhat familiar integral approach, assuming the form of the radial profiles, has been used.[1]

Over-all momentum, energy, and mass balances result in the following equations (assuming that the jet exit static pressure is equal to ambient pressure and that the exit profiles are flat):

$$\pi\int_0^\infty \rho u(u-u_\infty)d(r^2) = \rho_e u_e(u_e-u_\infty)\frac{\pi d^2}{4} \quad (1)$$

$$\pi\int_0^\infty \rho u\left[c(T-T_\infty)+\frac{J}{2}(u^2-u_\infty{}^2)\right]d(r^2) = \frac{\pi d^2}{4}\rho_e u_e\left[c_e(T_e-T_\infty)+\frac{J}{2}(u_e{}^2-u_\infty{}^2)+\Delta H_c\right] \quad (2)$$

$$\pi\int_0^\infty \frac{R-R_\infty}{R_e-R_\infty}\rho u d(r^2) = \pi\int_0^\infty \frac{c-c_\infty}{c_e-c_\infty}\rho u d(r^2) = \frac{\pi d^2}{4}\rho_e u_e \quad (3)$$

where c and R are the specific heat at constant pressure and the gas constant, respectively, and ΔH_c, the heat of combustion per pound of exhaust products, is included to account for gross effects due to afterburning (J = conversion factor). The following equations[2, 3] for the variation of the half-radius $r_{1/2}$ (radius at which the velocity defect, $u-u_\infty$, is half of that on the jet centerline),

$$\frac{r_{1/2}}{d} = C_1\left(\frac{x-a}{d}\right) \qquad \frac{u-u_\infty}{u_\infty} \gg 1 \quad (4a)$$

$$\frac{r_{1/2}}{d} = C_1\left(\frac{x-a}{d}\right)^{1/3} \qquad \frac{u-u_\infty}{u_\infty} \ll 1 \quad (4b)$$

coupled with radial profiles represented by the Gaussian error law,

$$\frac{u-u_\infty}{u_m-u_\infty} = \exp\left[-\left(\frac{r}{r_{1/2}}\right)^2 \ln 2\right] \quad (5)$$

$$\frac{T-T_\infty}{T_m-T_\infty} = \frac{R-R_\infty}{R_m-R_\infty} = \frac{c-c_\infty}{c_m-c_\infty} = \exp\left[-\frac{1}{n}\left(\frac{r}{r_{1/2}}\right)^2 \ln 2\right] \quad (6)$$

Received April 8, 1964.

* Senior Aerothermo Engineer, Engineering Sciences Branch. Associate Member AIAA.

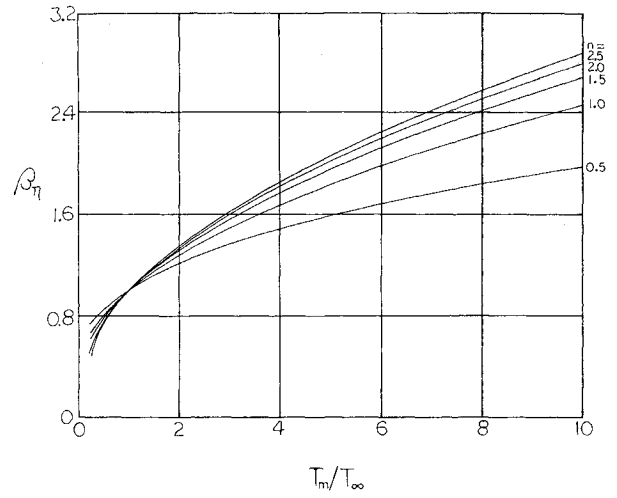

Fig. 1 Nonisothermal correction factor vs temperature ratio with n as a parameter.

yield

$$\frac{u-u_\infty}{u_m-u_\infty} = \exp\left[-\frac{\ln 2}{C_1{}^2}\left(\frac{r}{x-a}\right)^2\right] = \exp(-C_2\xi^2) \qquad \frac{u-u_\infty}{u_\infty} \gg 1 \quad (7a)$$

$$\frac{u-u_\infty}{u_m-u_\infty} = \exp\left[-\frac{\ln 2}{C_1{}^2}\left(\frac{x-a}{d}\right)^{4/3}\left(\frac{r}{x-a}\right)^2\right] = \exp\left[-C_2\left(\frac{x-a}{d}\right)^{4/3}\xi^2\right] \qquad \frac{u-u_\infty}{u_\infty} \ll 1 \quad (7b)$$

where $C_2 = (\ln 2)/C_1{}^2$ and $\xi = r/(x-a)$. Similar expressions for the scalar quantities in Eq. (1) result, except for the n, which accounts for the more rapid spread (i.e., $n > 1$) of the scalar quantities as compared to the momentum spread in free jet flow. It is to be noted that n is the reciprocal of the turbulent Prandtl number.

Because of space limitations, only case a for the velocity defect $u-u_\infty$ much larger than the freestream velocity U_∞ will be considered herein. Further results may be found in Ref. 1.

Substituting Eq. (7a), together with its scalar counterparts, into Eqs. (1–3), using the perfect gas law, rearranging, and integrating gives [neglecting the square of $u_\infty/(u_m-u_\infty)$ compared to unity in the energy equation] the following:

Momentum

$$\frac{u_m-u_\infty}{[u_e(u_e-u_\infty)]^{1/2}}\frac{x-a}{d} = \left[\frac{(C_2/2)(R_\infty T_\infty/R_e T_e)}{1+2(\beta_n{}^2/\beta^2{}_{n/2})[u_\infty/(u_m-u_\infty)]}\right]^{1/2}\beta_n \quad (8)$$

Energy

$$\frac{x-a}{d} = \frac{A}{2}\left[1+\left(1-\frac{4B}{A^2}\right)^{1/2}\right] \quad (9)$$

where

$$A = \frac{D}{2n\beta_n}\left[\left(\frac{C_2}{2}\right)\left(\frac{R_\infty T_\infty}{R_e T_e}\right)\left(\frac{u_e}{u_e-u_\infty}\right)\right]^{1/2}\times \frac{c_e}{c_\infty}\frac{T_e-T_\infty}{T_m-T_\infty}\left\{1+\frac{\Delta H_e}{c_e(T_e-T_\infty)}+\frac{Ju_e{}^2}{2c_e(T_e-T_\infty)}\left(1+2\frac{u_\infty{}^2}{u_e{}^2}-3\frac{u_\infty}{u_e}\right)\right\} \quad (9a)$$